


Sensory coding is impaired in rat absence epilepsy

Florian Studer^{1,2} , Emel Laghouati^{1,2}, Guillaume Jarre^{1,2}, Olivier David^{1,2}, Benoît Pouyatos^{1,2,3} and Antoine Depaulis^{1,2}

¹University Grenoble Alpes, Grenoble Institut des Neurosciences, GIN, Grenoble, France

²Inserm, U1216, Grenoble, France

³Present address: INRS, F-54519, Vandoeuvre Les Nancy, France

Edited by: Ole Paulsen & Vincenzo Marra

Key points

- Absence epilepsy is characterized by the occurrence of spike-and-wave discharges concomitant with an alteration of consciousness and is associated with cognitive comorbidities.
- In a genetic model of absence epilepsy in the rat, the genetic absence epilepsy rat from Strasbourg (GAERS), spike-and-wave discharges are shown to be initiated in the barrel field primary somatosensory cortex that codes whisker-related information, therefore playing an essential role in the interactions of rodents with their environment.
- Sensory-information processing is impaired in the epileptic barrel field primary somatosensory cortex of GAERS, with a delayed sensory-evoked potential and a duplicated neuronal response to whisker stimulation in *in vivo* extracellular recordings. Yet, GAERS present no defaults of performance in a texture discrimination task, suggesting the existence of a compensatory mechanism within the epileptic neuronal network.
- The results of the present study indicate that physiological primary functions are processed differently in an epileptic cortical network.

Abstract Several neurodevelopmental pathologies are associated with disorganized cortical circuits that may alter primary functions such as sensory processes. In the present study, we investigated whether the function of a cortical area is altered in the seizure onset zone of absence epilepsy, a prototypical form of childhood genetic epilepsy associated with cognitive impairments. We first combined *in vivo* multichannel electrophysiological recordings and histology to precisely localize the seizure onset zone in the genetic absence epilepsy rat from Strasbourg (GAERS). We then investigated the functionality of this epileptic zone using extracellular silicon probe recordings of sensory-evoked local field potentials and multi-unit activity, as well as a behavioural test of texture discrimination. We show that seizures in this model are initiated in the barrel field part of the primary somatosensory cortex and are associated with high-frequency oscillations. In this cortex, we found an increased density of parvalbumin-expressing interneurons in layer 5 in GAERS compared to non-epileptic Wistar rats. Its functional investigation revealed that sensory

Florian Studer received his Master's degree in Neuroscience from the University of Strasbourg. He recently received his PhD in Neuroscience from the University Grenoble Alpes, where he worked under the supervision of Antoine Depaulis at the Grenoble Institut for Neuroscience. During his PhD, he focused on the implication of neocortical neuronal networks in absence seizure generation and their impact on the physiology of the somatosensory cortex.



abilities of GAERS are not affected in a texture-discrimination task, whereas the intracortical processing of sensory-evoked information is delayed and duplicated. Altogether, these results suggest that absence seizures are associated with an increase of parvalbumin-inhibitory neurons, which may promote the functional relationship between epileptic oscillations and high-frequency activities. Our findings suggest that cortical circuits operate differently in the epileptic onset zone and may adapt to maintain their ability to process highly specialized information.

(Received 11 October 2018; accepted after revision 12 December 2018; first published online 13 December 2018)

Corresponding author Florian Studer: Grenoble Institut des Neurosciences, Chemin Fortuné Ferrini 38700, La Tronche, France. Email: florianstuder@yahoo.com

Introduction

The whisker-sensory system is crucial for the interactions of rodents with their environment. Accordingly, whisker-related information is processed by highly-organized neuronal circuits from the barrel-field primary somatosensory cortex (S1Bf) (Feldmeyer *et al.* 2013; Crochet *et al.* 2018). The information follows a canonical circuit involved in its integration, which has been described in several sensory areas (Douglas *et al.* 1989; Douglas & Martin, 1991; Lefort *et al.* 2009). In rodents, the S1Bf performs a fine coding of the amplitude and/or direction of each whisker's deflection, therefore allowing a precise detection of the texture encountered by the animals, (Bruno *et al.* 2003; Kremer *et al.* 2011; Estebanez *et al.* 2016; Kerekes *et al.* 2017). This specific organization develops during brain maturation (Bureau *et al.* 2004) and relies on spontaneous activation and experience (van der Bourg *et al.* 2017). Despite their role in physiological processes, neuronal circuits can also be involved in pathological processes, as shown in epilepsy (Epsztein *et al.* 2005; Feldt Muldoon *et al.* 2013).

Absence-epilepsy (AE) is characterized by recurrent absence seizures associated with spike-and-wave discharges (SWDs) initiated in the cortex (Holmes *et al.* 2004; Tucker *et al.* 2007) without structural or lesional origins (Berg *et al.* 2010). Yet, AE is associated with cognitive impairments (Caplan *et al.* 2008), although addressing their cause in the clinic remains difficult. Determining whether physiological functions are altered in non-traumatic epileptic networks is essential for understanding the pathophysiology of idiopathic epilepsies and associated comorbidities.

In a genetic model of AE, the genetic absence epilepsy rat from Strasbourg (GAERS) (Depaulis *et al.* 2016), we first showed that SWDs are initiated in the barrel field (S1Bf), the whisker-related part of the primary somatosensory (S1) cortex, in line with previous reports (Polack *et al.* 2007). Despite recurrent epileptic activities arising from sensory cortices, it is possible to record sensory-evoked potentials (SEPs) during inter-ictal periods in GAERS, as in human patients (Chipaux *et al.* 2013). However, it remains unknown whether sensory information is processed the same way in epileptic vs. non-epileptic cortex

or whether sensory coding needs to adjust in epileptic circuits, leading to specific comorbidities. Indeed, sensory information is treated by highly specialized neocortical circuits (Harris & Mrsic-Flogel, 2013) and pathological conditions such as Fragile-X syndrome have been shown to modify this coding, leading to sensory hypersensitivity (Zhang *et al.* 2014). We hypothesized that the S1Bf cortex of GAERS processes tactile information differently from that in non-epileptic rats, such that the physiological function is maintained, notwithstanding frequent SWDs. Accordingly, we investigated the intracortical sequence of sensory information across S1Bf cortical layers evoked by multiwhisker stimulations and, in parallel, analysed the ability of GAERS to discriminate textures.

Methods

Ethical approval

The investigators understand the ethical principles under which the journal operates and the work conducted in the present study complies with its animal ethics checklist. All protocols were approved by local Ethical Committees (Grenoble Institute of Neuroscience, La Tronche, France) and the French Ministry of Research (APAFIS#9761-201712514393900 v3) and experiments were carried out in accordance with European Union guidelines (directive 2010/63/EU). Adult GAERS male rats (aged 2–4 months old, $n = 29$) of the Grenoble colony and age-matched control Wistar rats ($n = 28$) (Charles River, L'Arbresle, France) were used to perform these experiments. They were maintained under a 12:12 h light/dark cycle with food and water available *ad libitum*.

Local field potential (LFP) recordings in freely-moving rats

Electrode implantation. Rats were stereotaxically implanted in the S1Bf with bipolar electrodes (Enamelled copper wire, diameter 220 μm ; Block, Verden, Germany) when they were anaesthetized with a mixture of xylazine (5–10 mg kg^{-1} i.p.; Rompun[®]; Centravet, Taden, France) and ketamine (40–100 mg kg^{-1} i.p.; Clorketam1000[®]; Vetoquinol, Lure, France). Incisions and compression

points were infiltrated with lidocaine (2%; Centravet). Stereotaxic co-ordinates were antero-posterior from bregma (AP): -2.5 mm; mediolateral: -5.5 mm; dorso-ventral: -2.5 mm (Paxinos & Watson, 2007). A stainless steel screw (diameter 1 mm) inserted over the cerebellum served as the reference electrode. All electrodes were soldered to a female microconnector (BLR150Z; Fischer Elektronik, Lüdenscheid, Germany) and secured on the head of the animal with dental cement.

Video-LFP recordings. After a post-surgery recovery period of 1 week, LFPs were acquired from freely-moving rats with a digital acquisition system (Coherence 3NT; Deltamed, Le Bouscat, France) with a sampling rate of 1024 Hz and analogue bandpass filtering between 1 and 256 Hz, synchronized with the video. Rats were recorded for 60 min. The occurrence of cortical discharges on LFP recordings was always confirmed with respect to the video.

LFP signal analysis. Spectral analysis of cortical discharges was performed using ImaGIN, an open source SPM toolbox for intracranial electroencephalograms (<https://f-tract.eu/software/imagin>) written in Matlab (The MathWorks, Natick, MA, USA) for Fast Fourier Transforms (FFT) of intracortical LFPs, as described previously (Pouyatos *et al.* 2016). To determine the functional link between SWDs and gamma oscillations, we quantified the cross-frequency coupling by phase-coupling analysis using Brainstorm (Tadel *et al.* 2011), which is freely available for download online under the GNU general public license (<http://neuroimage.usc.edu/brainstorm>).

FlexMEA and silicon probes recordings

Surgery. Rats were initially anaesthetized for surgery with ketamine and xylazine, as described above, and then immobilized with D-tubocurarine hydrochloride pentahydrate (0.4 mg kg⁻¹, i.p.; Sigma-Aldrich, Saint-Quentin-Fallavier, France) and artificially ventilated. They were maintained in a sedated state by repeated injections of fentanyl (1 µg kg⁻¹, i.p.; Janssen-Cilag, Issy Les Moulineaux, France). This preparation allows the recording of immobilized GAERS in a quiet-wakefulness state prone to SWD occurrence during which sensory-evoked responses of the barrel cortex are similar to wakefulness (Depaulis *et al.* 2016). A craniotomy over the S1 cortex allowed the insertion of either a FlexMEA (32 channels; Multichannel System, Reutlingen, Germany) subdurally ($n = 4$) or linear silicon probes (16 channels, 15 µm site, diameter 150 µm inter-site distance; Neuro-nexus Technologies, Ann Arbor, MI, USA) ($n = 12$). The insertion depth of the silicon probes was controlled via a micromanipulator. *Post hoc* detection of polarity reversion in infragranular layers (Kandel & Buzsáki, 1997) associated with DiI application on the back of the

probes was used to assess its location in cortical layers. During silicon probe recordings, a tin ECoG electrode was positioned on the dura mater near the silicon probe. For FlexMEA (i.e. flexible microelectrode array) recordings, LFP was amplified through a miniature preamplifier (MPA32; Multichannel System). For linear silicon probes recordings, the signal was amplified through two miniature preamplifiers (MPA8i, Multichannel System, Germany). For both types of electrodes, preamplifiers were connected to a 32-channel programmable gain amplifier (PGA-32, voltage gain, $\times 200$; Multichannel System) and sampled at 5 kHz (FlexMEA) or 20 kHz (silicon probes) (16 bit ADC). Recordings were collected on a personal computer via a CED interface (Cambridge Electronic Design, Cambridge, UK) using Spike 2 software (Cambridge Electronic Design).

SEPs. Sensory responses were evoked by air puffs (50 ms) timed by a pressure device (PMI-200; Dagan, Minneapolis, MN, USA) and delivered to the contralateral whiskers. Air puffs, which deflected four to eight whiskers by $\sim 10^\circ$ (Chipaux *et al.* 2013), were applied 60–100 times at 0.24 Hz. The principal whisker could not be detected precisely, although the orientation and pressure (10–20 psi) of the air puff was adjusted to generate a SEP of maximal amplitude (i.e. the most specific response) (Mahon & Charpier, 2012; Chipaux *et al.* 2013).

Signal analysis. The FlexMEA signal was analysed using the ImaGIN toolbox. SWDs were extracted from the raw signal and the h^2 coefficient of non-linear correlation was calculated for the total duration of SWDs (Lopes da Silva *et al.* 1989; Pijn *et al.* 1990; Meeren *et al.* 2002; Wendling *et al.* 2009) for each pair of electrodes of the array, aiming to estimate the strength and directionality of the association between all pairs of electrodes and detect the driving-electrodes during the SWDs. We then calculated the mean h^2 value for all comparisons of one single electrode as the h^2 output vs. input differences and obtained the mean directionality of the association for each electrode. Epileptogenicity Index (EI) analysis was also performed on the same data for the total duration of SWDs, as described previously (David *et al.* 2011). Briefly, a time-dependent FFT analysis of SWDs and their baseline was performed to measure spectral power over time. Baseline was chosen as period of at least 20 s without strong artefact before SWDs. EI, which is the Student's t value of the comparison of power between ictal and baseline periods, was computed for each electrode to estimate the strength of high frequency oscillations (60–400 Hz). Both h^2 and EI mean results for each electrodes were plotted on colour-coded maps and their comparison allowed the localization of the seizure onset zone.

Silicon probes raw signal was bandpass filtered (0.1–100 Hz) for current source density (CSD) analysis.

CSD was computed on each recording site as the second spatial derivative (Nicholson & Freeman, 1975) to detect extracellular sources and sinks in S1Bf layers using the formula: $D = \Phi(z - \Delta z) - 2\Phi(z) + \Phi(z + \Delta z)$, where Φ is the LFP, z is the vertical co-ordinate depth of the electrode and Δz is the inter-recording site distance. Accordingly, CSD calculation for the LFP of an electrode (x) takes into account the LFP signal from electrodes (x), ($x - 1$) and ($x + 1$). Therefore, we performed the CSD calculation for electrodes 2 to 15 from the 16-contacts silicon probe and obtain a 14-row CSD map. Multi-unit activity (MUA) was detected as negative event ≥ 2 SD of the baseline on the passband-filtered trace (0.6–6 kHz). LFP and MUA analysis were performed using custom-written Matlab scripts and Spike2 software (Cambridge Electronic Design).

Immunohistochemistry

Slice preparation and staining. Animals (aged 2–3 months old) were killed with an overdose of pentobarbital (200 mg kg⁻¹, i.p.) and transcardially perfused with PBS followed by 4% paraformaldehyde (PFA). Brains were collected, postfixed (4% PFA at 4°C, overnight), cryoprotected (30% sucrose at 4°C for 2 days), frozen in isopentane (−40°C for 1 min) and cut into coronal sections (40 μm thickness). Free-floating sections were saturated and permeabilized in 0.25% Triton X-100, 2% BSA in PBS (1 h at room temperature). Primary antibodies were incubated in PBS (4°C, overnight). The primary antibodies used were: anti-neuronal nuclei (NeuN; mouse; dilution 1:500; Merck Millipore, Billerica, MA, USA), anti-γ-amino-butyric acid (GABA; rabbit; dilution 1:250; Sigma-Aldrich), anti-parvalbumin (PV; mouse; dilution 1:500; Sigma-Aldrich) and anti-somatostatin (SOM; rabbit; dilution 1:250; BMA Biomedicals, Augst, Switzerland). After extensive washing in PBS, sections were incubated with appropriate species secondary antibodies conjugated to Alexa Fluor 488, 555 (dilution 1:500; Life Technologies, Grand Island, NY, USA) in the dark (2 h at room temperature) followed by 4',6-diamidino-2-phenylindole (DAPI) counterstaining (Hoechst; dilution 1:2000; 5 min at room temperature; Invitrogen, Carlsbad, CA, USA). Brain sections were extensively washed and mounted onto glass slides and coverslipped with anti-fading mounting medium (Aqua Poly/Mount; Polysciences, Inc., Warrington, PA, USA).

Image analysis. Confocal images were acquired using an inverted confocal microscope (LSM 710; Carl Zeiss, Oberkochen, Germany). Cellular counting was performed manually using ImageJ (NIH, Bethesda, MD, USA) in the S1Bf based on the expression of specific markers (NeuN, GABA, PV) on slices randomly chosen within co-ordinates between −2 mm and −3 mm from bregma (Paxinos

& Watson, 2007). Supragranular (2/3), granular (4) and infragranular (5 and 6) layers were separated based on DAPI and/or NeuN staining over a 5 μm thick image stack. The areas of layers 2/3, 4, 5 and 6 were measured with Fiji (NIH). For each animal ($n = 5$ per group), we estimated the cell density in four different slices and the average of five values was used for statistical comparison between groups.

Texture discrimination task

This test was adapted from the discrimination task used in mice (Wu *et al.* 2013; Chen *et al.* 2018) and the novelty recognition task developed for rats (Ennaceur & Delacour, 1988). It is specific to whisker-related information processing because whiskers and S1Bf have to be intact for the rat to be able to perform correctly (Wu *et al.* 2013; Chen *et al.* 2018). The protocol and its timeline are shown in Fig. 5A. This test was carried-out in an arena (50 × 50 × 50 cm). On day 1, rats were individually habituated to the arena for 10 min. On day 2, two columns (5 × 6 × 9 cm) with identical textures were placed in opposite corners of the arena. Each rat was placed in the centre of the arena and left for 5 min of habituation to the textured columns (encoding phase). The rat was then put back into its home cage for 5 min (consolidation phase). The two columns were replaced by one column with the same texture as that used during the encoding phase and one with a new texture. The rat was allowed 3 min to explore the new columns (testing phase). The textures were composed of 50 and 120 grit sandpapers (Diall; Templemars, France), chosen as the difference allowing the best discrimination in rodents (Wu *et al.* 2013). The location of the columns and the 50 and 120 grit sandpaper were randomly selected as habituated or novel textures to avoid biases. The tests were video recorded and analysed by an observer who was blind to the animal strains. The exploration of the two textures was determined as approaches with the nose of the rat in a 4 cm width area around the columns. The discrimination index was calculated as the ratio of the difference of time spent exploring the two columns with respect to the total exploration time. The time that rats spent touching the object with their body was not counted. Rats were included in the analysis only if they spent more than 10 s of total exploration during each phase.

Locomotion and anxiety-like behaviour tests

Rats were individually placed in an open arena (50 × 100 cm) artificially divided in a central zone (25 × 75 cm) and an external zone corresponding to a 12.5 cm stripe between the central zone and the wall of the arena. The test was recorded using a video tracking system (ViewPoint, Lyon, France). The locomotion was quantified as the total

distance travelled during the 10 min of the test. The number of entries and the total time spent in the central zone were quantified to evaluate anxiety-like behaviour.

Statistical analysis

Statistical analysis was performed using Prism, version 7 (GraphPad Software, San Diego, CA, USA). Comparison between experimental groups was performed using a non-parametric Mann–Whitney test unless otherwise mentioned. Data are reported as the mean \pm SEM. $P \leq 0.05$ was considered statistically significant.

Results

SWDs are initiated in the S1Bf cortex in GAERS

Several studies performed in two genetic models of absence epilepsy (i.e. GAERS and WAG/Rij) have shown that SWDs are initiated in the primary somatosensory cortex (S1) (Meeren *et al.* 2002; Polack *et al.* 2007; David *et al.* 2008) and suggested that SWD are generated in the oro-facial part of this region (Meeren *et al.* 2002; Polack *et al.* 2007). S1 LFP recordings are characterized by the presence of SWDs (Fig. 1A) coherent with an increased LFP power between 4 and 10 Hz, as well as between 40 and 80 Hz (Fig. 1B). This increased power was significant in the SWD frequency band (6–8 Hz) (Fig. 1B). The increase in the gamma frequency band (40–60 Hz) was concomitant with the 6–8 Hz LFP power elevation of SWDs (Fig. 1C). Those oscillations (i.e. SWD and gamma) are functionally related, as highlighted by their phase–amplitude coupling relationship during SWDs (Fig. 1D).

To better localize the cortical area initiating SWDs, we used a 32 channel subdural FlexMEA placed on the surface of the cortex in adult GAERS to cover unilaterally a large cortical area (6 \times 4 mm), including the S1 and adjacent cortices (i.e. motor, parietal and part of the auditory cortices). To determine where SWDs first arise, we calculated the h^2 coefficient (Lopes da Silva *et al.* 1989; Meeren *et al.* 2002; Wendling *et al.* 2009), a non-linear correlation index between all pairs of electrodes that allows the identification of driving electrodes during the seizure (i.e. the epileptic onset zone) ($n = 4$ rats, $n = 80$ SWDs). We found the highest h^2 coefficient in the primary S1, with a hot spot in the S1Bf, and a progressive decrease from S1 to M1 cortex (Fig. 1E, left). We took advantage of the functional link between SWDs and gamma oscillations (Fig. 1D) to confirm the h^2 results with the EI, commonly used in the clinic (Bartolomei *et al.* 2008; David *et al.* 2011; Roehri *et al.* 2017) (Fig. 1E, right). This analysis indicated that the highest EI was also found in the S1Bf.

Our data confirm the localization of the SWD generator in the S1 in GAERS and further suggest that SWDs are specifically initiated in the S1Bf.

Inhibitory interneurons are increased in the S1Bf of GAERS

Based on the functional interaction between SWDs and gamma oscillations (Fig. 1D) and the known role of PV+ and SOM+ interneurons in gamma oscillation generation (Buzsáki *et al.* 1983; Traub *et al.* 1996; Mann *et al.* 2005; Cardin *et al.* 2009; Sohal *et al.* 2009; Veit *et al.* 2017), we hypothesized that GAERS could present a layer-specific increase of interneurons density, especially of PV+ or SOM+ cells. Recent studies indicated modifications of GABAergic interneurons densities in models of genetic epilepsy that further support our hypothesis (Wimmer *et al.* 2015; Papp *et al.* 2018). NeuN staining for neurons did not show significant difference in neuronal density between GAERS and Wistar controls (Fig. 2A and B). However, GABA staining (Fig. 2A) and PV staining (Fig. 2D) for inhibitory interneurons revealed a significant increase of interneurons density in layer 5 in GAERS (Fig. 2C and E), whereas the density of SOM+ (Fig. 2D) was significantly increased in layer 4 in GAERS (Fig. 2F).

Our data obtained in the GAERS reveal an increase of SOM-expressing interneurons in layer 4 and PV-expressing interneurons in layer 5 of S1Bf, which is the same layer that has been suggested to initiate spikes during SWDs.

SEPs are delayed in GAERS

Because the S1Bf of GAERS generates SWDs and presents an increased density of interneurons, we hypothesized that its function (i.e. coding and integration of sensory information mediated by the whiskers) would be impaired. To examine whether the S1Bf of GAERS codes whisker-mediated information as in Wistar rats, we first analysed the characteristics of the peak of ECoG-recorded SEPs (i.e. latency and amplitude) after whisker stimulations by air puff in immobilized rats (Fig. 3A and B). Although the peak amplitudes of SEPs were not significantly different between GAERS and Wistar rats (GAERS: $382 \pm 51 \mu\text{V}$, Wistar: $276 \pm 80 \mu\text{V}$; Mann–Whitney test, $P = 0.43$) (Fig. 3D), we observed a significantly longer latency in GAERS (GAERS: 52 ± 3.7 ms, Wistar: 35.8 ± 3.2 ms; Mann–Whitney test, $P \leq 0.05$) (Fig. 3C).

We further examined whether sensory stimuli were processed by the S1Bf circuit in GAERS with the same canonical sequence (L4 \rightarrow L2/3 \rightarrow L5/6) as in Wistar. Accordingly, we recorded LFP activity among cortical layers using multichannel silicon probes (Fig. 3A) and analysed the evoked intracortical SEPs by CSD analysis to determine the sequence of activity upon air puff stimulation. In Wistar rats, in L4, we first observed a sink associated with a local source, which was followed by a similar dipole in L2/3 and then in L5, in agreement with

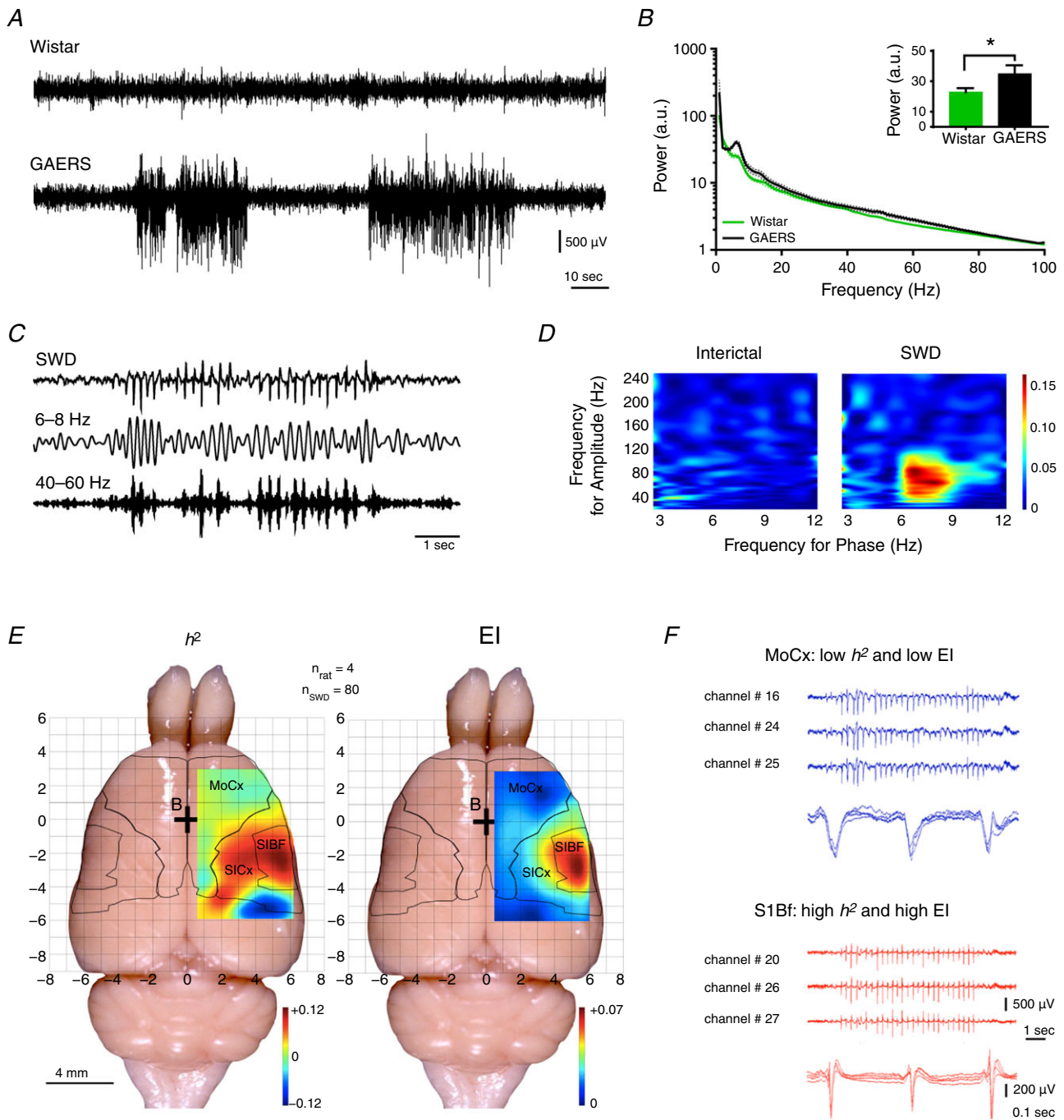


Figure 1. SWDs initiating zone localization in the S1Bf cortex

A, examples of LFP recordings in the S1 cortex in freely moving Wistar rat (top) and GAERS (bottom). **B**, FFT power of 60 min LFP recordings in freely moving GAERS and Wistar (mean \pm SEM; $n = 4$ per group). Inset: mean \pm SEM 6–8 Hz power ($n = 4$ per group; $*P \leq 0.05$, Mann–Whitney test). **C**, example of trace of a SWD recorded in the S1 cortex of a GAERS (top) filtered to highlight increased power in the 6–8 Hz (middle) and 40–60 Hz (bottom) frequency bands. **D**, example of phase–amplitude coupling maps of interictal and ictal (SWD) LFP recordings. **E**, h^2 (left) and EI (right) mean colour-coded maps of 32-contact FlexMEA recorded SWDs (rats, $n = 4$; SWDs, $n = 80$). **F**, raw trace examples of FlexMEA recordings in the motor cortex (MoCx, blue) and in the S1Bf (red) with each time an enlargement of three successive spike- and waves.

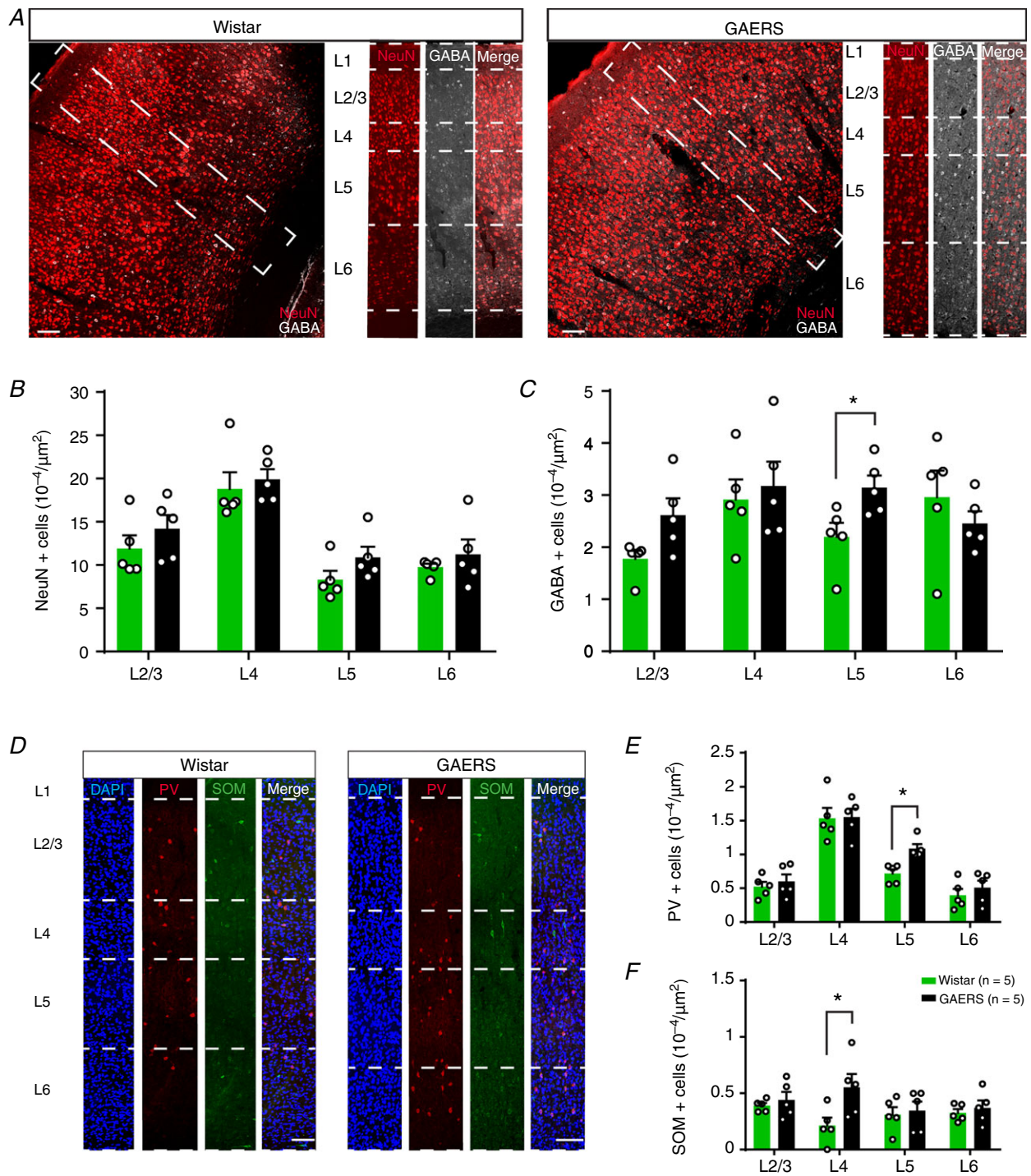


Figure 2. Neuronal densities of the S1Bf cortex

A, example of coronal sections of the S1Bf cortex of Wistar (left) and GAERS (right) with NeuN (red) and GABA (grey) immunostaining. Dashed squares delineate insets. Dashed lines delineate cortical layers. B, quantification of the mean density of NeuN+ among S1Bf cortical layers cells ($n = 6002$ and 7029 cells for Wistar and GAERS, respectively). C, quantification of the mean density of GABA+ interneurons among S1Bf cortical layers ($n = 1350$ and 1577 cells for Wistar and GAERS, respectively). D, example immunostaining of DAPI (blue), PV (red) and SOM (green) among S1Bf cortical layers for Wistar (left) and GAERS (right). E, quantification of the mean density of PV+ interneurons among S1Bf cortical layers ($n = 356$ and 448 cells for Wistar and GAERS, respectively). F, quantification of the mean density of SOM+ interneurons among S1Bf cortical layers ($n = 181$ and 223 cells for Wistar and GAERS, respectively). Scale bars = $100 \mu\text{m}$ (mean \pm SEM; $n = 5$ rats per group; open circles represents one rat; $*P \leq 0.05$, Mann-Whitney test).

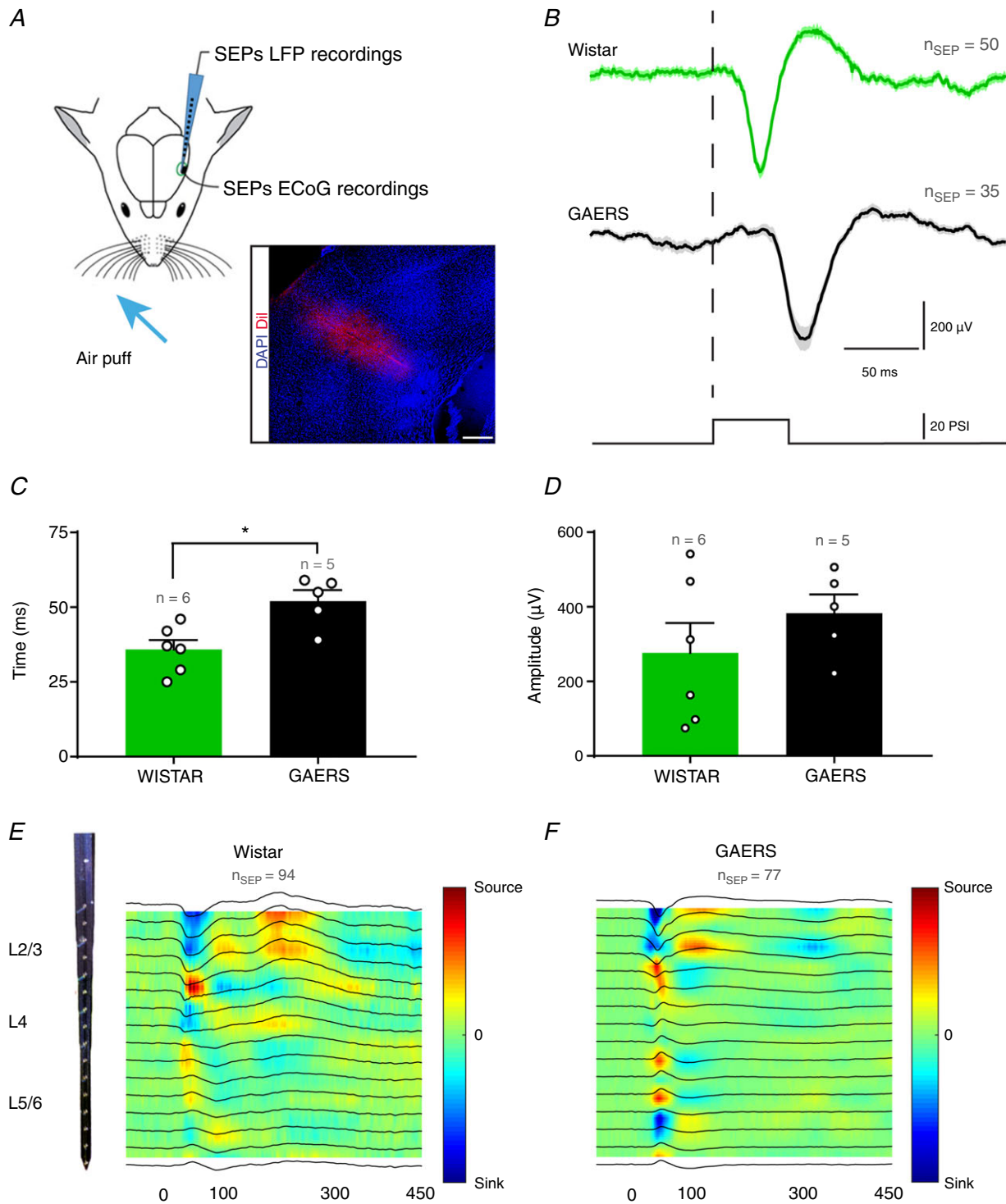


Figure 3. Sensory-evoked LFP activity in the S1Bf

A, schematic drawing of the experimental preparation allowing air puff induced SEP recordings over S1Bf in immobilized rats. Inset: Dil trace of the silicon probe in the S1Bf. Scale bar = 400 μm . **B**, example traces of SEP evoked in Wistar (green) and GAERS (black) (mean \pm SEM; $n \geq 35$ SEPs per group). Dashed line indicates the onset of 50 ms air puff stimulation. **C** and **D**, quantification of the latency and amplitude of the peak of SEP after air puff stimulation (mean \pm SEM; $n = 6$ and 5 for Wistar (green) and GAERS (black) respectively; open circles represents one rat; $*P \leq 0.05$, Mann-Whitney test). **E** and **F**, examples of CSD maps of average SEP among cortical layers with 16-contact linear silicon probes. Corresponding LFP traces are overlaid over colour maps ($n = 6$ rats per group, $n \geq 35$ SEPs; linear colour code scale).

the canonical circuit (Reyes-Puerta *et al.* 2015; van der Bourg *et al.* 2017) (Fig. 3E). In GAERS, we observed a similar sequence, although with a delay of a few milliseconds, as for EcoG, comprising a weak sink in L4 associated with a positive LFP deflection not observed in Wistar rats and with a more pronounced dipole of current (i.e. more local activity) in L5/6 compared to Wistar controls (Fig. 3F). In addition, we observed a sink ~ 300 ms after whisker stimulation (Fig. 3F), suggesting an increased neuronal activation, especially in L2/3 neurons in GAERS, which was not observed in Wistar rats. In both groups, CSD analysis revealed higher sinks in supra- and infragranular layers, most probably because of the multiwhisker stimulation activating the paralemniscal pathway (Lübke & Feldmeyer, 2007).

Our data suggest that sensory information are processed in the S1Bf of GAERS via the canonical circuit, although the evoked responses are delayed compared to Wistar controls.

Neuronal-evoked activity is delayed and duplicated in GAERS

To confirm the LFP sequence of activation after multiwhisker stimulation, we further analysed the response to air puff delivery on neuronal MUA among cortical layers of the S1Bf (Fig. 4A). As expected, in Wistar and GAERS, we observed an increase of MUA within the first 150 ms following the stimulation as indicated by the grand-average peristimulus time histograms (PSTH) representing the mean activity among cortical layers (Fig. 4B). The peak response during these first 150 ms was at 30 ms for Wistar rats, whereas GAERS presented a significant delay in all layers (Fig. 4B and C), with comparable coefficient of variations (69% vs. 64% in L2/3, 56% vs. 48% in L4, 49% vs. 49% in L5/6 for Wistar and GAERS, respectively) and in line with our EcoG results and CSD analysis. The mean activity among cortical layers was ~ 120 Hz in Wistar rats but only 80 Hz in GAERS in all layers (Fig. 4B). Z scored PSTH maps confirmed the peaks of activity and further described the selective response of neurons to whisker stimulation among cortical layers (Fig. 4D). The MUA evoked within the first 150 ms was significantly decreased in L4 in GAERS compared to Wistar rats (Holm–Sidak test, $P \leq 0.05$) (Fig. 4E) and the activity at the first peak was significantly decreased in all layers (Holm–Sidak test, $P \leq 0.05$) (Fig. 4F). This suggests that the response to the stimulation was less selective and less synchronized in GAERS than in Wistar rats. This synchronized activation observed at the peak in Wistar rats was followed by a post-activity depression not observed in GAERS. However, in GAERS, we observed a second and higher peak (280–340 ms) (Fig. 4B and D), in coherence with the observed late sink on the CSD map (Fig. 3F). There, the MUA increase appeared to occur first in L5

(Fig. 4D, right). This second peak appeared specific to GAERS because no change of MUA was detected in Wistar rats (Fig. 4B, D and G). Notably, L5 neurons in GAERS displayed a continuous high-frequency activity that was not present in Wistar rats (data not shown), in line with our previous observations (Polack *et al.* 2007).

The results of the present study show that the neuronal activity evoked in S1Bf by whisker stimulation is different in GAERS compared to Wistar controls. Although the sequence of neuronal activations across layers in GAERS follows the canonical circuit, their response during the first 150 ms is blurrier than that in Wistar rats, which present a more significant MUA increase at the early peak (10–50 ms), suggesting a higher selectivity to whisker stimulation (van der Bourg *et al.* 2017). Our MUA data also confirmed the delay in the neuronal response to air puff, which could be a result of the increased inhibition suggested above by the increased density of PV+ and SOM+ neurons in S1Bf, as well as the existence of a second phase of neuronal activity ~ 250 ms after the first one.

GAERS rats are able to discriminate between textures

Although sensory processing in GAERS involves the canonical circuit in the S1Bf cortex, the delayed and secondary responses to whisker stimulation suggested that their ability to discriminate between textures could be affected. Therefore, we investigated whether sensory integration was efficient in GAERS using a behavioural test of texture discrimination (Fig. 5A) in which the integrity of the whisker-related pathway of sensory processing is mandatory (Wu *et al.* 2013; Chen *et al.* 2018). In this test, both GAERS and Wistar rats were able to discriminate between the two proposed textures because they spent more time exploring the new texture during the testing phase (Fig. 5B–D) (Wilcoxon signed rank test against 50% chance, $P \leq 0.05$). Moreover, we found no differences between the performances of GAERS and Wistar rats in this task (Mann–Whitney test, $P = 0.47$) (Fig. 5E). Importantly, this test was specific to whisker-related signalling because GAERS were no better able to discriminate after whisker trimming (data not shown), in line with previous reports (Wu *et al.* 2013; Chen *et al.* 2018).

To confirm that these results were not biased by a decreased locomotion and/or increased anxiety-like behaviour, as suggested by previous studies with respect to GAERS (Jones *et al.* 2008), we monitored the locomotor activity of GAERS and Wistar rats in an open field (50 \times 100 cm) (Fig. 6A). The total distance travelled during 10 min was not different between the two groups (Mann–Whitney test, $P = 0.4$) (Fig. 6B). GAERS spent significantly more time in the central area and entered significantly more frequently in this zone (Fig. 6C), suggesting a reduced anxiety-like behaviour in GAERS

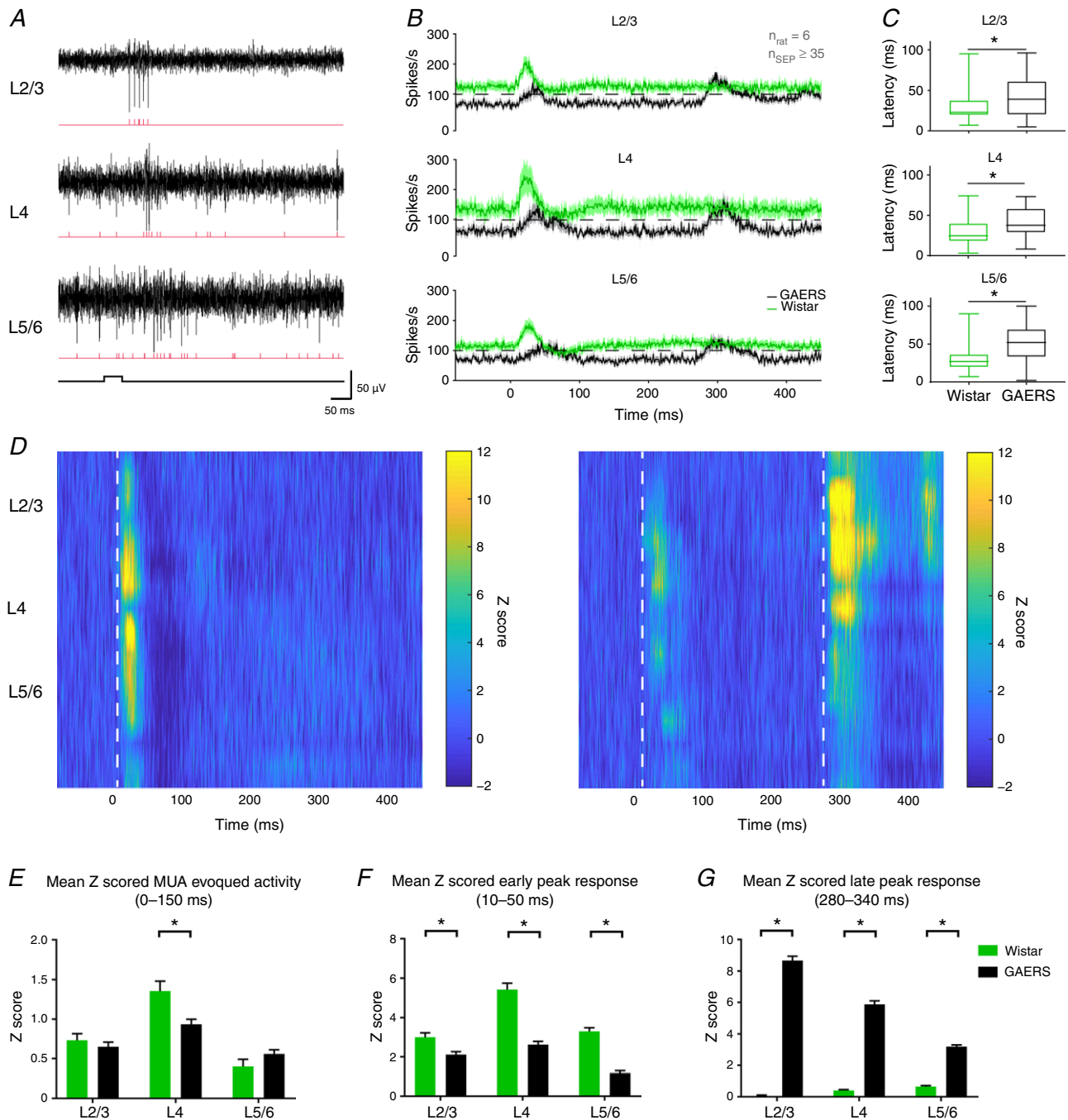


Figure 4. MUA-evoked activity in the S1Bf cortex

A, example traces of MUA (black) recorded in the S1Bf during whisker stimulation and corresponding raster plots (red). B, grand average PSTH among cortical layers. Dashed lines represent 100 spikes s^{-1} . C, box plot distribution of MUA peak activation latency among cortical layers ($*P \leq 0.05$, Mann–Whitney test). D, Z scored PSTH of MUA activity with respect to the cortical layers for Wistar (left) and GAERS (right). Dashed lines highlight the beginning of MUA-evoked activity. E, quantification of the MUA-evoked activity between 0 and 150 ms after the onset of air puff stimulation in Wistar (green) and GAERS (black). F, quantification of the MUA-evoked activity activity between 10–50 ms after the onset of air puff stimulation in Wistar (green) and GAERS (black). G, quantification of the MUA-evoked activity between 280 and 340 ms after the onset of air puff stimulation in Wistar (green) and GAERS (black) (mean \pm SEM; $n = 6$ rats per group, $n \geq 35$ SEPs per group; $*P \leq 0.05$, Holm–Sidak test).

compared to Wistar controls. Moreover, no seizures were observed on the video in GAERS during the time spent in the central area. Finally, using the rotarod test, we observed no difference in sensory-motor co-ordination between GAERS and Wistar rats (Mann–Whitney test, $P = 0.8$) (Fig. 6E).

Our behavioural data suggest that, despite the critical involvement of S1Bf in SWD initiation and the changes observed in sensory-evoked activity processing, GAERS are nonetheless able to integrate whisker-related sensory information.

Discussion

Understanding the link between altered physiological functioning and seizures in idiopathic epilepsies is essential for unravelling and taking better care of associated comorbidities in human patients. In this respect, sensory processing that involves specific neocortical circuits to allow a refined coding of information from the environment is probably altered in an epileptic cortex. In the present study, we showed that, despite the

presence of abnormal neuronal activities and populations, sensory circuits of S1Bf from GAERS rats were still able to process whisker-related information. Indeed, we showed that GAERS are able to integrate and remember thin texture differences and also that the intracortical processing involves the canonical circuit, as in Wistar rats. However, our data also revealed a delay in this information processing and the existence of a neuronal activity reverberation in GAERS.

Characterizing the physiopathology of the seizure onset zone

In the present study, it was important to precisely locate the site of seizure initiation in the S1 cortex of GAERS and perform depth recordings within the exact site that drives SWDs to test its specific function. Accordingly, we compared the results obtained with h^2 and EI analysis, which are two methodologies that have already been used to identify seizure onset zones in animal models (Meeren *et al.* 2002) and patients (David *et al.* 2011; Roehri *et al.* 2017). The h^2 map, which results from

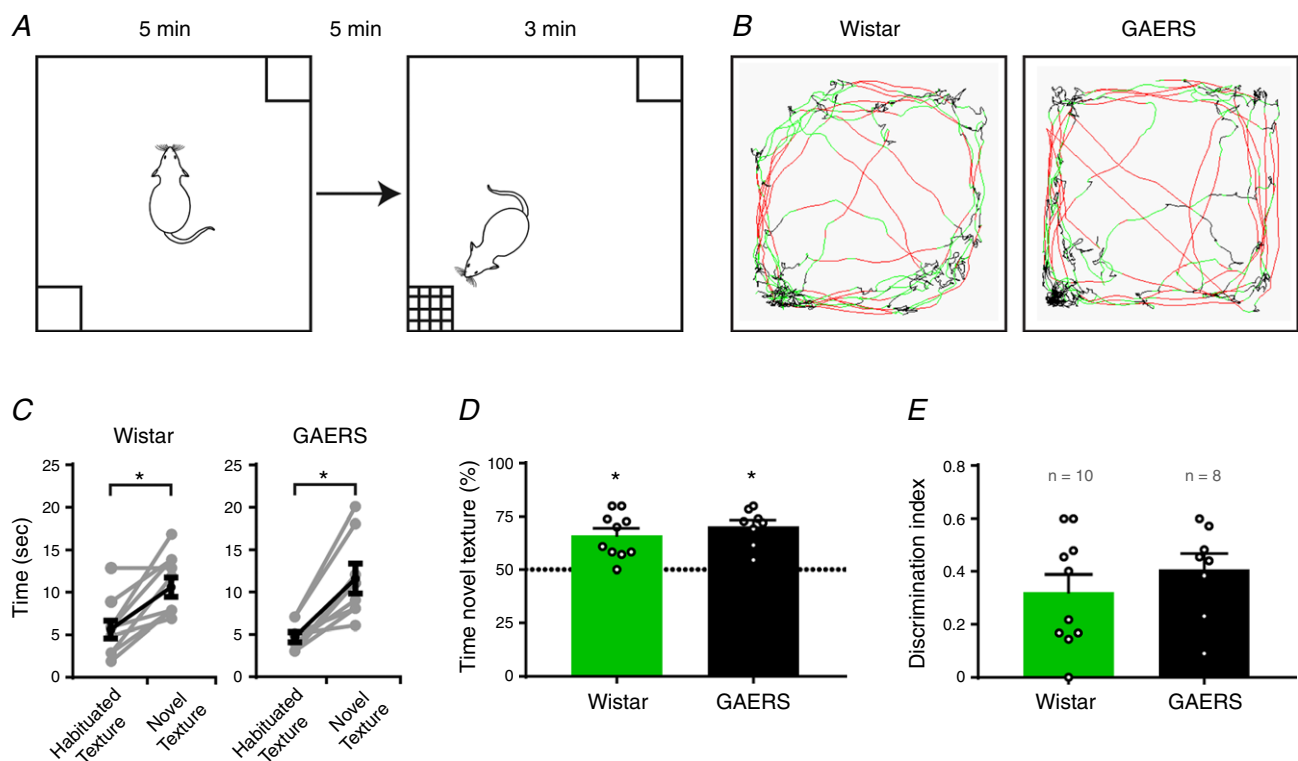
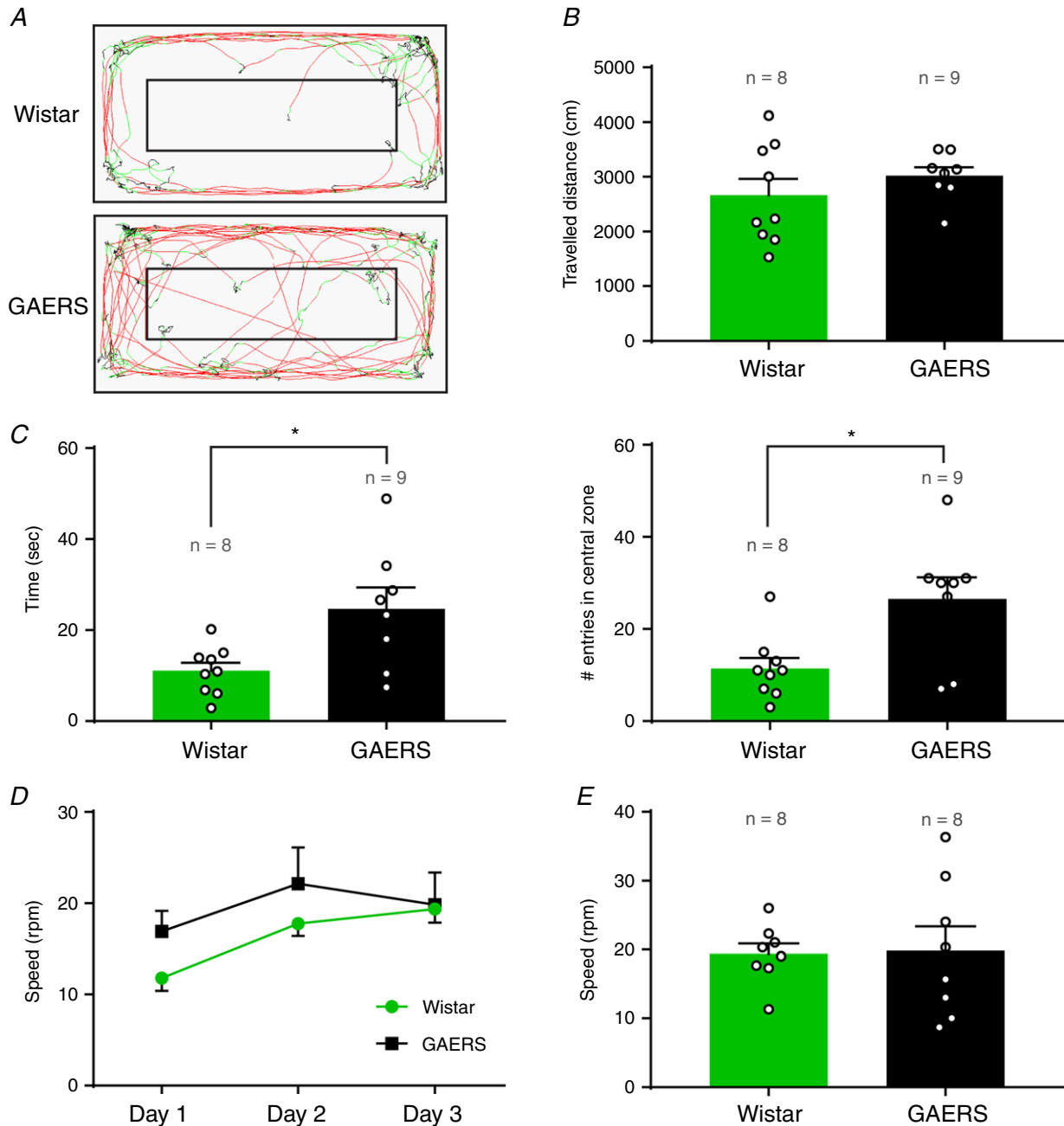


Figure 5. Texture discrimination evaluation

A, schematic representation of the experimental design for the discrimination task. B, example traces of the locomotion of rats during the test (red: fast movements; green: slow movements; black: immobility). In these examples, the novel texture was in the bottom left. C, quantification of the exploration time for both textures during the test phase (each paired dot represents one rat; * $P \leq 0.05$, Wilcoxon test). D, quantification of the percentage of time spent exploring the novel texture. Dashed line represents 50% chance (* $P \leq 0.05$, Wilcoxon signed rank test against 50% chance). E, quantification of the index of discrimination (n.s., Mann–Whitney test) (mean \pm SEM; $n = 10$ and 8 for Wistar (green) and GAERS (black), respectively; open circles represent one rat).

the average of directionality comparisons between pairs of electrodes, was less focal than the EI map, which takes into account only the local dynamic activity of each electrode. Although each method has its limitations (Roehri *et al.* 2017), they both highlighted the S1Bf as the site of SWD initiation among the different cortical

regions explored with FlexMEA. Because S1Bf codes for whisker activity (Bruno *et al.* 2003; Estebanez *et al.* 2016), these data further raised the issue of a possible alteration of the neuronal circuits involved in sensory processes in GAERS. We therefore evaluated the capacity of sensory integration in GAERS. With this aim, we



chose a spontaneous discrimination task because, as a non-associative test, it does not require any training of the rats and is not dependent on motivational aspects or learning processes (Grayson *et al.* 2015). This is important, especially in AE, which has been shown to be associated with such comorbidities in patients (Caplan *et al.* 2008). This choice was also motivated by data suggesting that GAERS present an anhedonic behaviour, as indicated in the sucrose preference test (Jones *et al.* 2008). This could have been a confounding factor in associative tests where motivation can be critical. Because an increase of anxiety-like behaviour has also been described in GAERS (Jones *et al.* 2008) that could have influenced our discrimination test, we also examined the time spent in the central area of an open space. Our data rather indicate a reduced fear in GAERS compared to Wistar rats, in line with the results reported in previous studies (Vergnes *et al.* 1991; Marques-Carneiro *et al.* 2014).

Potential role of GABAergic inhibition in sensory impairment

Even though the sensory integration did not appear to be affected in GAERS, we provide electrophysiological evidence suggesting that sensory coding is processed differently in these animals. Indeed, whisker stimulation induced delayed evoked responses in GAERS compared to Wistar rats both on LFP and MUA. This delay could be the result of interference regarding the pathological circuit with the canonical circuit in S1Bf. Especially, our immunolabelling data revealed an increased GABAergic density in the S1Bf network in GAERS, suggesting an enhanced inhibition that could at least partly explain the delayed response after whisker deflection. Because PV+ and SOM+ interneurons are essential for sensory coding and gamma oscillation (Cardin *et al.* 2009; Buzsáki & Wang, 2012; Veit *et al.* 2017), an increased number of these interneurons could explain the augmented gamma power in GAERS that not only favours SWDs, but also may alter sensory coding. A recent study showed no difference in terms of GABA+ interneurons in the S1Bf of GAERS (Bombardi *et al.* 2018). By contrast, another recent study showed an elevation of PV+ interneurons in the S1 cortex of GAERS that was not present in WAG/Rij (Papp *et al.* 2018). As was suggested, this could reflect the difference in epileptogenesis time-course between the two models of AE: because SWDs appear later in WAG/Rij (3 months *vs.* 3 weeks in GAERS) (Jarre *et al.* 2017), the increase of PV+ cells in GAERS could result from the repetition of SWDs. This suggests that the increased density of inhibitory interneurons could rather be a consequence of the repetition of seizures than its cause. However, the cellular migration of interneurons should be finished before the appearance of SWDs in GAERS (Wonders & Anderson, 2006), therefore suggesting that their increased density

could rather participate, at least indirectly, in the initiation of SWD by promoting the pro-epileptogenic activities of high-frequency oscillations (Cardin *et al.* 2009; Veit *et al.* 2017). In this case, comorbidities associated with AE could partly result from the plasticity induced by seizure recurrence, as suggested recently (Bombardi *et al.* 2018). If this hypothesis is confirmed in the clinic, it raises the need to detect and block absence seizures as soon as possible in patients. This increased inhibitory activity is in line with previous data suggesting an increased GABAergic tone in GAERS (Cope *et al.* 2009; Chipaux *et al.* 2011), as well as a greater sensitivity to GABAergic analogues (Vergnes *et al.* 1984). It remains to be examined whether the impairment of some subunits of GABA_A receptor observed in these animals also participates in the delay of sensory processing (Spreafico *et al.* 1993).

Duplicated sensory-induced neuronal response in the epileptic cortex

The most striking result that we collected in the present study is the existence in GAERS of a second wave of neuronal activity. This reverberation of response could allow a better encoding of the sensory information, as reported in other sensory cortices (Bermudez Contreras *et al.* 2013; Rothschild *et al.* 2017). This is coherent with the fact that the response elicited during the first 100 ms following whisker stimulation is less important in GAERS compared to Wistar rats, suggesting a decreased neuronal selectivity to sensory stimulation. This second wave could be caused by a retro control inside the epileptogenic thalamocortical loop. Indeed, corticothalamic neurons activated by the whisker stimulation could activate inhibitory neurons from the thalamic reticular nucleus, in turn inducing a rebound activation of thalamocortical neurons (Buzsáki, 1991; Pinault *et al.* 2001; Pinault, 2003) that can initiate the subsequent secondary wave of cortical MUA onto the hyperexcitable neurons from S1Bf in the GAERS (Polack *et al.* 2007). This same second wave of MUA could also be triggered by a feedback activity coming from the motor cortex that is essential to sensory integration and accurate perception (Manita *et al.* 2015). Our data suggest that this second wave is generated in L5, a finding that is in agreement with recent studies showing that neurons of this layer are able to synchronize the cortical column and generate cortical waves (Stroh *et al.* 2013). It is also in agreement with our previous data showing that deep layer neurons are hyperexcitable in the GAERS (Polack *et al.* 2007). We propose that the hyperexcitability of neurons in the deep layers could favour the reverberation of the sensory information upon the initial activation (Bermudez Contreras *et al.* 2013). Whether this intense second wave compensates the less selective and synchronized initial response and allows

GAERS to maintain efficient whisker-mediated tactile performances remains to be examined. Indeed, GAERS are able to discriminate textures, in coherence with previous studies showing normal evoked responses in these animals (Chipaux *et al.* 2013). Our data, performed in adult GAERS, cannot determine whether the changes that we observed are a result of the repetition of generalized seizures rather than the building up of the epileptogenic circuit.

Conclusions

Altogether our results highlight the interference of epileptic networks on physiological processes but also suggest the existence of neuroplasticity processes that may arise to compensate the subsequent impairments. In human patients, AE has been shown to be associated with cognitive comorbidities such as attentional deficits and speech defaults (Caplan *et al.* 2008; Glauser *et al.* 2010). Whether these comorbidities are associated with an impairment of the neural circuit in the frontal cortex suggested to be one of the main seizure onset zone (Holmes *et al.* 2004; Tucker *et al.* 2007) requires further investigation. Compensatory processes, as suggested by our data in rats, may also occur in young patients preserving them from serious crippling comorbidities.

References

- Bartolomei F, Chauvel P & Wendling F (2008). Epileptogenicity of brain structures in human temporal lobe epilepsy: a quantified study from intracerebral EEG. *Brain* **131**, 1818–1830.
- Berg AT, Berkovic SF, Brodie MJ, Buchhalter J, Cross JH, Van Emde Boas W, Engel J, French J, Glauser TA, Mathern GW, Moshé SL, Nordli D, Plouin P & Scheffer IE (2010). Revised terminology and concepts for organization of seizures and epilepsies: report of the ILAE Commission on Classification and Terminology, 2005–2009. *Epilepsia* **51**, 676–685.
- Bermudez Contreras EJ, Schjetnan AGP, Muhammad A, Bartho P, McNaughton BL, Kolb B, Gruber AJ & Luczak A (2013). Formation and reverberation of sequential neural activity patterns evoked by sensory stimulation are enhanced during cortical desynchronization. *Neuron* **79**, 555–566.
- Bombardi C, Venzi M, Crunelli V & Di Giovanni G (2018). Developmental changes of GABA immunoreactivity in cortico-thalamic networks of an absence seizure model. *Neuropharmacology* **136**, 56–67.
- van der Bourg A, Yang J-W, Reyes-Puerta V, Laurency B, Wieckhorst M, Stüttgen MC, Luhmann HJ & Helmchen F (2017). Layer-specific refinement of sensory coding in developing mouse barrel cortex. *Cereb Cortex* **27**, 4835–4850.
- Bruno RM, Khatri V, Land PW & Simons DJ (2003). Thalamocortical angular tuning domains within individual barrels of rat somatosensory cortex. *J Neurosci Off J Soc Neurosci* **23**, 9565–9574.
- Bureau I, Shepherd GM & Svoboda K (2004). Precise development of functional and anatomical columns in the neocortex. *Neuron* **42**, 789–801.
- Buzsáki G (1991). The thalamic clock: emergent network properties. *Neuroscience* **41**, 351–364.
- Buzsáki G, Leung LW & Vanderwolf CH (1983). Cellular bases of hippocampal EEG in the behaving rat. *Brain Res* **287**, 139–171.
- Buzsáki G & Wang X-J (2012). Mechanisms of gamma oscillations. *Annu Rev Neurosci* **35**, 203–225.
- Caplan R, Siddarth P, Stahl L, Lanphier E, Vona P, Gurbani S, Koh S, Sankar R & Shields WD (2008). Childhood absence epilepsy: behavioral, cognitive, and linguistic comorbidities. *Epilepsia* **49**, 1838–1846.
- Cardin JA, Carlén M, Meletis K, Knoblich U, Zhang F, Deisseroth K, Tsai L-H & Moore CI (2009). Driving fast-spiking cells induces gamma rhythm and controls sensory responses. *Nature* **459**, 663–667.
- Chen C-C, Lu J, Yang R, Ding JB & Zuo Y (2018). Selective activation of parvalbumin interneurons prevents stress-induced synapse loss and perceptual defects. *Mol Psychiatry* **23**, 1614–1625.
- Chipaux M, Charpier S & Polack P-O (2011). Chloride-mediated inhibition of the ictogenic neurones initiating genetically-determined absence seizures. *Neuroscience* **192**, 642–651.
- Chipaux M, Vercueil L, Kaminska A, Mahon S & Charpier S (2013). Persistence of cortical sensory processing during absence seizures in human and an animal model: evidence from EEG and intracellular recordings. *PLoS ONE* **8**, e58180.
- Cope DW, Giovanni GD, Fyson SJ, Orbán G, Errington AC, Lőrincz ML, Gould TM, Carter DA & Crunelli V (2009). Enhanced tonic GABA_A inhibition in typical absence epilepsy. *Nat Med* **15**, 1392.
- Crochet S, Lee S-H & Petersen CCH (2018). Neural circuits for goal-directed sensorimotor transformations. *Trends Neurosci* **42**, 66–77.
- David O, Blauwblomme T, Job A-S, Chabardès S, Hoffmann D, Minotti L & Kahane P (2011). Imaging the seizure onset zone with stereo-electroencephalography. *Brain* **134**, 2898–2911.
- David O, Guillemain I, Sallet S, Rey S, Deransart C, Segebarth C & Depaulis A (2008). Identifying neural drivers with functional MRI: an electrophysiological validation *PLoS Biol* **6**, e315.
- Depaulis A, David O & Charpier S (2016). The genetic absence epilepsy rat from Strasbourg as a model to decipher the neuronal and network mechanisms of generalized idiopathic epilepsies. *J Neurosci Methods* **260**, 159–174.
- Douglas RJ & Martin KA (1991). A functional microcircuit for cat visual cortex. *J Physiol* **440**, 735–769.
- Douglas RJ, Martin KAC & Whitteridge D (1989). A canonical microcircuit for neocortex. *Neural Comput* **1**, 480–488.
- Ennaceur A & Delacour J (1988). A new one-trial test for neurobiological studies of memory in rats. 1: Behavioral data. *Behav Brain Res* **31**, 47–59.
- Epszstein J, Represa A, Jorquera I, Ben-Ari Y & Crépel V (2005). Recurrent mossy fibers establish aberrant kainate receptor-operated synapses on granule cells from epileptic rats. *J Neurosci* **25**, 8229–8239.

- Estebanez L, Bertherat J, Shulz DE, Bourdieu L & Léger J-F (2016). A radial map of multi-whisker correlation selectivity in the rat barrel cortex. *Nat Commun* **7**, 13528.
- Feldmeyer D, Brecht M, Helmchen F, Petersen CCH, Poulet JFA, Staiger JF, Luhmann HJ & Schwarz C (2013). Barrel cortex function. *Prog Neurobiol* **103**, 3–27.
- Feldt Muldoon S, Soltesz I & Cossart R (2013). Spatially clustered neuronal assemblies comprise the microstructure of synchrony in chronically epileptic networks. *Proc Natl Acad Sci U S A* **110**, 3567–3572.
- Glauser TA, Cnaan A, Shinnar S, Hirtz DG, Dlugos D, Masur D, Clark PO, Capparelli EV & Adamson PC (2010). Ethosuximide, valproic acid, and lamotrigine in childhood absence epilepsy. *N Engl J Med* **362**, 790–799.
- Grayson B, Leger M, Piercy C, Adamson L, Harte M & Neill JC (2015). Assessment of disease-related cognitive impairments using the novel object recognition (NOR) task in rodents. *Behav Brain Res* **285**, 176–193.
- Harris KD & Mrsic-Flogel TD (2013). Cortical connectivity and sensory coding. *Nature* **503**, 51–58.
- Holmes MD, Brown M & Tucker DM (2004). Are ‘generalized’ seizures truly generalized? evidence of localized mesial frontal and frontopolar discharges in absence. *Epilepsia* **45**, 1568–1579.
- Jarre G, Altwegg-Boussac T, Williams MS, Studer F, Chipaux M, David O, Charpier S, Depaulis A, Mahon S & Guillemain I (2017). Building up absence seizures in the somatosensory cortex: from network to cellular epileptogenic processes. *Cereb Cortex* **27**, 4607–4623.
- Jones NC, Salzberg MR, Kumar G, Couper A, Morris MJ & O’Brien TJ (2008). Elevated anxiety and depressive-like behavior in a rat model of genetic generalized epilepsy suggesting common causation. *Exp Neurol* **209**, 254–260.
- Kandel A & Buzsáki G (1997). Cellular–synaptic generation of sleep spindles, spike-and-wave discharges, and evoked thalamocortical responses in the neocortex of the rat. *J Neurosci* **17**, 6783–6797.
- Kerekes P, Daret A, Shulz DE & Ego-Stengel V (2017). Bilateral discrimination of tactile patterns without whisking in freely running rats. *J Neurosci* **37**, 7567–7579.
- Kremer Y, Léger J-F, Goodman D, Brette R & Bourdieu L (2011). Late emergence of the vibrissa direction selectivity map in the rat barrel cortex. *J Neurosci* **31**, 10689–10700.
- Lefort S, Tomm C, Floyd Sarria J-C & Petersen CCH (2009). The excitatory neuronal network of the C2 barrel column in mouse primary somatosensory cortex. *Neuron* **61**, 301–316.
- Lopes da Silva F, Pijn JP & Boeijinga P (1989). Interdependence of EEG signals: linear vs. nonlinear associations and the significance of time delays and phase shifts. *Brain Topogr* **2**, 9–18.
- Lübke J & Feldmeyer D (2007). Excitatory signal flow and connectivity in a cortical column: focus on barrel cortex. *Brain Struct Funct* **212**, 3–17.
- Mahon S & Charpier S (2012). Bidirectional plasticity of intrinsic excitability controls sensory inputs efficiency in layer 5 barrel cortex neurons in vivo. *J Neurosci Off J Soc Neurosci* **32**, 11377–11389.
- Manita S, Suzuki T, Homma C, Matsumoto T, Odagawa M, Yamada K, Ota K, Matsubara C, Inutsuka A, Sato M, Ohkura M, Yamanaka A, Yanagawa Y, Nakai J, Hayashi Y, Larkum ME & Murayama M (2015). A top-down cortical circuit for accurate sensory perception. *Neuron* **86**, 1304–1316.
- Mann EO, Suckling JM, Hajos N, Greenfield SA & Paulsen O (2005). Perisomatic feedback inhibition underlies cholinergically induced fast network oscillations in the rat hippocampus in vitro. *Neuron* **45**, 105–117.
- Marques-Carneiro JE, Faure J-B, Cosquer B, Koning E, Ferrandon A, de Vasconcelos AP, Cassel J-C & Nehlig A (2014). Anxiety and locomotion in Genetic Absence Epilepsy Rats from Strasbourg (GAERS): inclusion of Wistar rats as a second control. *Epilepsia* **55**, 1460–1468.
- Meeren HKM, Pijn JPM, Van Luijtelaar ELJM, Coenen AML & Lopes da Silva FH (2002). Cortical focus drives widespread corticothalamic networks during spontaneous absence seizures in rats. *J Neurosci Off J Soc Neurosci* **22**, 1480–1495.
- Nicholson C & Freeman JA (1975). Theory of current source-density analysis and determination of conductivity tensor for anuran cerebellum. *J Neurophysiol* **38**, 356–368.
- Papp P, Kovács Z, Szocsics P, Juhász G & Maglóczy Z (2018). Alterations in hippocampal and cortical densities of functionally different interneurons in rat models of absence epilepsy. *Epilepsy Res* **145**, 40–50.
- Paxinos G & Watson C (2007). The Rat Brain in Stereotaxic Coordinates, 6th edn. Available at: <https://www.elsevier.com/books/the-rat-brain-in-stereotaxic-coordinates/paxinos/978-0-12-374121-9> [Accessed 22 November 2017].
- Pijn JPM, Vijn PCM, Lopes da Silva FH, Van Ende Boas W & Blanes W (1990). Localization of epileptogenic foci using a new signal analytical approach. *Neurophysiol Clin Neurophysiol* **20**, 1–11.
- Pinault D (2003). Cellular interactions in the rat somatosensory thalamocortical system during normal and epileptic 5–9 Hz oscillations. *J Physiol* **552**, 881–905.
- Pinault D, Vergnes M & Marescaux C (2001). Medium-voltage 5–9-Hz oscillations give rise to spike-and-wave discharges in a genetic model of absence epilepsy: in vivo dual extracellular recording of thalamic relay and reticular neurons. *Neuroscience* **105**, 181–201.
- Polack P-O, Guillemain I, Hu E, Deransart C, Depaulis A & Charpier S (2007). Deep layer somatosensory cortical neurons initiate spike-and-wave discharges in a genetic model of absence seizures. *J Neurosci* **27**, 6590–6599.
- Pouyatos B, Nemoz C, Chabrol T, Potez M, Bräuer E, Renaud L, Pernet-Gallay K, Estève F, David O, Kahane P, Laissue JA, Depaulis A & Serduc R (2016). Synchrotron X-ray microtransections: a non invasive approach for epileptic seizures arising from eloquent cortical areas. *Sci Rep* **6**, 27250.
- Reyes-Puerta V, Sun J-J, Kim S, Kilb W & Luhmann HJ (2015). Laminar and columnar structure of sensory-evoked multineuronal spike sequences in adult rat barrel cortex in vivo. *Cereb Cortex* **25**, 2001–2021.
- Roehri N, Pizzo F, Lagarde S, Lambert I, Nica A, McGonigal A, Giusiano B, Bartolomei F & Bénar C-G (2017). High-frequency oscillations are not better biomarkers of epileptogenic tissues than spikes. *Ann Neurol* **83**, 84–97.

- Rothschild G, Eban E & Frank LM (2017). A cortical–hippocampal–cortical loop of information processing during memory consolidation. *Nat Neurosci* **20**, 251–259.
- Sohal VS, Zhang F, Yizhar O & Deisseroth K (2009). Parvalbumin neurons and gamma rhythms enhance cortical circuit performance. *Nature* **459**, 698–702.
- Spreafico R, Mennini T, Danober L, Cagnotto A, Regondi MC, Miari A, De Blas A, Vergnes M & Avanzini G (1993). GABAA receptor impairment in the genetic absence epilepsy rats from Strasbourg (GAERS): an immunocytochemical and receptor binding autoradiographic study. *Epilepsy Res* **15**, 229–238.
- Stroh A, Adelsberger H, Groh A, Rühlmann C, Fischer S, Schierloh A, Deisseroth K & Konnerth A (2013). Making waves: initiation and propagation of corticothalamic Ca²⁺ waves in vivo. *Neuron* **77**, 1136–1150.
- Tadel F, Baillet S, Mosher JC, Pantazis D & Leahy RM (2011). Brainstorm: a user-friendly application for MEG/EEG analysis. *Comput Intell Neurosci* **2011**, <https://doi.org/10.1155/2011/879716>.
- Traub RD, Whittington MA, Stanford IM & Jefferys JGR (1996). A mechanism for generation of long-range synchronous fast oscillations in the cortex. *Nature* **383**, 621–624.
- Tucker DM, Brown M, Luu P & Holmes MD (2007). Discharges in ventromedial frontal cortex during absence spells. *Epilepsy Behav* **11**, 546–557.
- Veit J, Hakim R, Jadi MP, Sejnowski TJ & Adesnik H (2017). Cortical gamma band synchronization through somatostatin interneurons. *Nat Neurosci* **20**, 951–959.
- Vergnes M, Marescaux C, Boehrer A & Depaulis A (1991). Are rats with genetic absence epilepsy behaviorally impaired? *Epilepsy Res* **9**, 97–104.
- Vergnes M, Marescaux C, Micheletti G, Depaulis A, Rumbach L & Warter JM (1984). Enhancement of spike and wave discharges by GABA-mimetic drugs in rats with spontaneous petit-mallike epilepsy. *Neurosci Lett* **44**, 91–94.
- Wendling F, Ansari-Asl K, Bartolomei F & Senhadji L (2009). From EEG signals to brain connectivity: a model-based evaluation of interdependence measures. *J Neurosci Methods* **183**, 9–18.
- Wimmer VC, Li MY-S, Berkovic SF & Petrou S (2015). Cortical microarchitecture changes in genetic epilepsy. *Neurology* **84**, 1308–1316.
- Wonders CP & Anderson SA (2006). The origin and specification of cortical interneurons. *Nat Rev Neurosci* **7**, 687–696.
- Wu H-PP, Ioffe JC, Iverson MM, Boon JM & Dyck RH (2013). Novel, whisker-dependent texture discrimination task for mice. *Behav Brain Res* **237**, 238–242.
- Zhang Y, Bonnan A, Bony G, Ferezou I, Pietropaolo S, Ginger M, Sans N, Rossier J, Oostra B, LeMasson G & Frick A (2014). Dendritic channelopathies contribute to neocortical and sensory hyperexcitability in *Fmr1*^{-/-} mice. *Nat Neurosci* **17**, 1701–1709.

Additional information

Competing interests

The authors declare that they have no competing interests.

Author contributions

FS, GJ and AD took part in the conception and design of the research. FS, EL and BP performed the data acquisition. FS, BP and OD performed the data analysis. FS, BP and AD participated in the interpretation of data. FS and AD drafted the manuscript and prepared the figures. EL, GJ, OD and BP revised and improved the manuscript. All authors approved the final version of the manuscript submitted for publication and agree to be accountable for all aspects of the work. All persons designated as authors qualify for authorship, and all those who qualify for authorship are listed.

Funding

This work was supported by funding from the *Institut National de la Santé et de la Recherche Médicale* (INSERM) and grants from the *Agence Nationale de la Recherche* (ANR, ‘EPIRAD’ #13-BSV1-0012-01 2013 and ‘SoAbsence’ #16-CE37-0021 2016). FS received support from the *Ligue Française contre l’Épilepsie* and the Grenoble Alpes University.

Acknowledgements

We thank S. Andrieu, C. Colomb and all of the staff of the GIN animal facility for providing animal care. We thank also S. Carnicella for his advice regarding the behavioural tests, as well as L. Vercueil and I. Guillemain for their comments on the manuscript.